Generation of multicolored tripartite entanglement by frequency doubling in a two-port resonator

Rongguo Yang, Shuqin Zhai, Kui Liu, Junxiang Zhang, and Jiangrui Gao*

State Key Laboratory of Quantum Optics and Quantum Optics Devices, Institute of Opto-Electronics, Shanxi University, Taiyuan 030006, China
**Corresponding author: jrgao@sxu.edu.cn*

Received May 12, 2010; revised October 12, 2010; accepted October 13, 2010; posted October 18, 2010 (Doc. ID 128400); published November 18, 2010

Multicolored multipartite entanglement is of great importance in quantum communication and quantum information networks. In this paper, we calculate the quantum fluctuations of the fundamental frequency pump beam and second-harmonic beams in a two-port frequency doubling resonator, and investigate the tripartite continuous-variable entanglement generated by this device for the first time, to our knowledge. The quantum correlation among fundamental frequency pump beam and two harmonic beams is studied using a necessary and sufficient criterion for Gaussian entanglement states, the positivity under partial transposition. It is found that two-color tripartite entanglement exists in a large range of pump intensities and analysis frequencies.

OCIS codes: 270.0270, 270.6570, 190.2620.

Entanglement, which is probably the most special one of all the quantum phenomena, is considered to be the basic resource of quantum information processing. Experimental and theoretical works about bipartite entanglement were performed in diverse systems, such as optical parametric amplifier or optical parametric oscillator [1,2], combination of two squeezed lights with a beam splitter [3], and frequency doubling in a resonator with two output ports [4,5]. The bipartite entanglement has already been applied in quantum teleportation [6–8], dense coding [9], cryptography [10], and tomography of state [11]. Now, entanglement between more than two parties is going to be the key ingredient for advanced quantum communication, for example, quantum teleportation network [12], telecloning [13,14], and controlled dense coding [15,16]; and the multipartite entangled beams with different frequencies will be more important since it will be necessary for the quantum networks and the message storage, in which the wavelengths are connected with fiber window, air window, and different atom transition lines. Research on the multicolored multipartite quantum entanglement has been developed. The generation of continuous-variable tripartite entanglement by cascaded nonlinear interaction has been proposed theoretically in an optical parametric oscillator cavity with parametric downconversion and sum-frequency [17]. Villar *et al.* demonstrated theoretically that the quantum entanglement exists among the three output fields (pump, signal, and idler) of a triply resonant nondegenerate optical parametric oscillator operating above threshold [18]. Zhai *et al.* then demonstrated the tripartite entanglement in a process of type-II second-order harmonic generation (SHG) with a triply resonant optical cavity [19,20]. Furthermore two- and three-color optical quantum correlations have been observed, respectively, in experiment recently by Grosse *et al.* and Coelho *et al.* [21,22]. They opened a way of generating the multicolored entangled beams.

In this paper we report a generation of tripartite quantum entanglement with two frequencies in the SHG process with a dual-port cavity. The quantum correlations among the fundamental frequency field and two output harmonic beams are discussed versus the pump intensity and analysis frequency using the positivity under partial transposition (PPT) criterion.

Figure 1 shows the dual-ported SHG cavity that can provide two harmonic outputs and a fundamental frequency field. The cavity is resonant at the fundamental frequency, and both mirrors are transparent for the second-harmonic field. The pump fundamental frequency beam enters the cavity at the input-output coupler 1 and oscillates in cavity. The forward fundamental frequency field traverses the crystal from left to right; thus one harmonic field (SH1) is generated and output completely at coupler 2, indicated as output 1. Then the backward fundamental frequency field traverses the crystal from right to left in cavity, and the second-harmonic field (SH2) is generated. Both the output fundamental frequency field and a second-harmonic field (SH2) are output at coupler 1, indicated as output 2. Both second-harmonic waves SH1 and SH2 are generated by the same fundamental frequency field in forward and backward processes, respectively; they are correlated with each other and also correlated with fundamental wave under appropriate conditions.

The intra-cavity fundamental frequency and harmonic field are self-consistent at the steady state condition, and

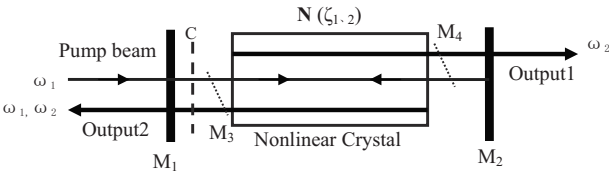

Fig. 1. Dual-port cavity of single resonant SHG: Output1, one harmonic field; Output2, the other harmonic field and the reflect pump field.

the intra-cavity field annihilation operators at the right of input-output coupler 1 $\hat{a}_{iC}$ can be written as

$$\hat{a}_{iC}(t+\tau) = \mathbf{r_1}\mathbf{t}_4^L N(\zeta_2)\mathbf{r}_2\mathbf{t}_3^L N(\zeta_1)\hat{a}_{iC}(t) + \mathbf{t}_1\hat{b}_{i1}(t) + \mathbf{r_1}\mathbf{t}_4^L N(\zeta_2)\mathbf{t_2}\hat{b}_{i2}(t) - \mathbf{r_1}\mathbf{t}_4^L N(\zeta_2)\mathbf{r_2}\mathbf{r}_3^L\hat{b}_{i3}(t) - \mathbf{r_1}r_4^L\hat{b}_{i4}(t). \quad (1)$$

Here $i=1,2$ are the corresponding fundamental and harmonic frequency fields, respectively, and these subscripts are used in the whole paper. $\hat{b}_{ij}(t)$ are the annihilation operators of vacuum for frequency i at mirror j ($j=1,2$ correspond to couplers 1 and 2, respectively, while $j=3,4$ correspond to residual intra-cavity losses due to the absorption of the crystal and the reflections at crystal two surfaces, respectively; these subscripts are also used in the whole paper). τ is a cavity round trip time. Nonzero diagonal elements of the 4×4 matrix for two output couplers' transmission and reflection are quoted as

$$\mathbf{t}_j = \mathrm{diag}(\sqrt{T_{1j}}, \sqrt{T_{2j}}, \sqrt{T_{1j}}, \sqrt{T_{2j}}), \quad (2a)$$

$$\mathbf{r}_j = \mathrm{diag}(\sqrt{1-T_{1j}}, \sqrt{1-T_{2j}}, \sqrt{1-T_{1j}}, \sqrt{1-T_{2j}}). \quad (2b)$$

Here T_{ij} denote the power transmittance for frequency i at mirror j. $N(\zeta_i)$ is the transformation matrix of single-pass traversing the crystal; it embodies a gain in second-harmonic generation with arbitrary interaction length ζ_i [23–25]. The expressions of $N(\zeta_i)$ are given in Appendix A [23,24]. The interaction length ζ_i can be given by $\zeta_1 = [(n_1/n_2)\sqrt{\varepsilon_1 E_{\mathrm{NL1}} P_{in}}]^{1/2}$, $\zeta_2 = [(n_1/n_2)\sqrt{\varepsilon_2 E_{\mathrm{NL2}} P_{in}}]^{1/2}$. Here we have introduced conversion efficiencies $\varepsilon_1 = P_{21}/P_{in}$, $\varepsilon_2 = P_{22}/P_{in}$. P_{21} and P_{22} are the harmonic powers generated by forward and backward fundamental frequency waves, respectively, and P_{in} is the fundamental frequency pump power. E_{NL1} and E_{NL2} are the single-pass conversion efficiencies of two second-harmonic waves, respectively, which can be measured in experiment. n_1 (n_2) is the fundamental (second-harmonic) refractive index. Residual intra-cavity losses are described by coefficients L_{ij}, which are taken into account as vacuum introduced by the artificial ports (beam splitters 3 and 4) at two ends of the crystal, and corresponding to the transmission and reflection matrices (t_j^L, r_j^L) are defined as

$$\mathbf{t}_j^L = \mathrm{diag}(\sqrt{1-L_{1j}}, \sqrt{1-L_{2j}}, \sqrt{1-L_{1j}}, \sqrt{1-L_{2j}}), \quad (3a)$$

$$\mathbf{r}_j^L = \mathrm{diag}(\sqrt{L_{1j}}, \sqrt{L_{2j}}, \sqrt{L_{1j}}, \sqrt{L_{2j}}). \quad (3b)$$

The Fourier transforms of Eq. (1) are $\hat{a}(t+\tau) \rightleftharpoons \hat{a}(\omega)e^{i\omega\tau}$, $\hat{a}(t) \rightleftharpoons \hat{a}(\omega)$. So we obtain the steady state self-consistent equation in the frequency domain:

$$\hat{a}_{iC}(\omega)e^{i\omega\tau} = \mathbf{r_1}\mathbf{t}_4^L N(\zeta_2)\mathbf{r}_2\mathbf{t}_3^L N(\zeta_1)\hat{a}_{iC}(\omega) + \mathbf{t}_1\hat{b}_{i1}(\omega) + \mathbf{r_1}\mathbf{t}_4^L N(\zeta_2)\mathbf{t_2}\hat{b}_{i2}(\omega) - \mathbf{r_1}\mathbf{t}_4^L N(\zeta_2)\mathbf{r_2}\mathbf{r}_3^L\hat{b}_{i3}(\omega) - \mathbf{r_1}r_4^L\hat{b}_{i4}(\omega). \quad (4)$$

Using the definitions of the amplitude and phase quadratures,

$$x_{iC}(\omega) = a_{ic}(\omega) + a_{ic}^*(\omega), \quad y_{iC}(\omega) = -i[a_{ic}(\omega) - a_{ic}^*(\omega)],$$

$$u_{ij}(\omega) = b_{ij}(\omega) + b_{ij}^*(\omega), \quad v_{ij}(\omega) = -i[b_{ij}(\omega) - b_{ij}^*(\omega)], \quad (5)$$

we can get the amplitude and phase quadratures of all fields. As the components, the amplitude and phase quadratures of the fundamental frequency and harmonic fields can form the vector $\mathbf{X}_C = (x_{1C}, x_{2C}, y_{1C}, y_{2C})^T$. The amplitude and phase quadratures of vacuum at mirror j correspond to the vector $\mathbf{v}_j = (u_{1j}(\omega), u_{2j}(\omega), v_{1j}(\omega), v_{2j}(\omega))^T$. ω is the analysis frequency. With these definitions and assumption, Eq. (4) can be written as

$$\mathbf{X}_C = D\mathbf{r_1}\mathbf{t}_4^L N(\zeta_2)\mathbf{r}_2\mathbf{t}_3^L N(\zeta_1)\mathbf{X}_C + D[\mathbf{t}_1\mathbf{v}_1 + \mathbf{r_1}\mathbf{t}_4^L N(\zeta_2)\mathbf{t_2}\mathbf{v}_2 - \mathbf{r_1}\mathbf{t}_4^L N(\zeta_2)\mathbf{r_2}\mathbf{r}_3^L\mathbf{v}_3 - \mathbf{r_1}\mathbf{r}_4^L\mathbf{v}_4], \quad (6)$$

where we have introduced a diagonal matrix $D = \mathrm{diag}(e^{-i\omega/v_{c1}}, e^{-i\omega/v_{c2}}, e^{-i\omega/v_{c1}}, e^{-i\omega/v_{c2}})$ which means the phase shift acquired in one cavity round trip. Here $v_{ci} = 1/\tau = c/(2L_{\mathrm{Cavity}} + 2n_i L_{\mathrm{crystal}})$ is the cavity free spectral range, c is the speed of light in vacuum, L_{Cavity} is the length of air in the cavity, L_{crystal} is the length of the crystal, and $i=1,2$ correspond to the fundamental frequency and SHG, respectively.

The vector of output quadratures is defined as

$$\mathbf{X}_j = (X_{1j}, X_{2j}, Y_{1j}, Y_{2j})^T. \quad (7)$$

Using boundary condition, the output quadratures can be written as

$$\mathbf{X}_1 = \mathbf{t}_2\mathbf{t}_3^L N(\zeta_1)\mathbf{X}_C - \mathbf{r}_2\mathbf{v}_2 - \mathbf{t}_2\mathbf{r}_3^L\mathbf{v}_3, \quad (8)$$

$$\mathbf{X}_2 = \mathbf{t}_1\mathbf{X_C}/D\mathbf{r}_1 - \mathbf{v}_1/\mathbf{r}_1. \quad (9)$$

In the case of single resonant fundamental frequency, the second harmonic transmits completely at output couplers, i.e., $T_{21}=T_{22}=1$ and $T_{12}=0$, and the intra-cavity losses of fundamental frequency fields L_{13} and L_{14} at mirrors 3 and 4 are nonzero, but the harmonic loss can be neglected, which means $L_{23}=L_{24}=0$. In fact, all harmonic losses can be merged with the detectors. Finally, the output harmonic quadratures, i.e., the element in the vector $\mathbf{X}_j$ derived from Eqs. (8) and (9), can be written as

$$X_{21}(\omega) = f_{11}u_{11}(\omega) + f_{13}u_{13}(\omega) + f_{14}u_{14}(\omega) + f_{21}u_{21}(\omega) + f_{22}u_{22}(\omega), \quad (10a)$$

$$Y_{21}(\omega) = g_{11}v_{11}(\omega) + g_{13}v_{13}(\omega) + g_{14}v_{14}(\omega) + g_{21}v_{21}(\omega) + g_{22}v_{22}(\omega), \quad (10b)$$

$$X_{22}(\omega) = h_{11}u_{11}(\omega) + h_{13}u_{13}(\omega) + h_{14}u_{14}(\omega) + h_{21}u_{21}(\omega) + h_{22}u_{22}(\omega), \quad (10c)$$

$$Y_{22}(\omega) = k_{11}v_{11}(\omega) + k_{13}v_{13}(\omega) + k_{14}v_{14}(\omega) + k_{21}v_{21}(\omega) + k_{22}v_{22}(\omega). \tag{10d}$$

$$X_{12}(\omega) = m_{11}u_{11}(\omega) + m_{13}u_{13}(\omega) + m_{14}u_{14}(\omega) + m_{21}u_{21}(\omega) + m_{22}u_{22}(\omega), \tag{10e}$$

$$Y_{12}(\omega) = n_{11}v_{11}(\omega) + n_{13}v_{13}(\omega) + n_{14}v_{14}(\omega) + n_{21}v_{21}(\omega) + n_{22}v_{22}(\omega). \tag{10f}$$

The coefficients (f,g,h,k) have been given in [4], and they are shown here again in Appendix A. The coefficients m and n are calculated as

$$m_{11} = \frac{e^{i\Omega/v_{c1}}\sqrt{1-L_{13}}\sqrt{1-L_{14}} - \sqrt{1-T_{11}}}{F}, \tag{11a}$$

$$m_{13} = -\frac{\sqrt{L_{13}}\sqrt{1-L_{14}}N_{11}(\zeta_2)\sqrt{T_{11}}}{F}, \tag{11b}$$

$$m_{14} = -\frac{\sqrt{L_{14}}\sqrt{T_{11}}}{F}, \tag{11c}$$

$$m_{21} = \frac{e^{iw/v_{c2}}\sqrt{1-L_{13}}\sqrt{1-L_{14}}N_{11}(\zeta_2)N_{12}(\zeta_1)\sqrt{T_{11}}}{F}, \tag{11d}$$

$$m_{22} = \frac{\sqrt{1-L}N_{12}(\zeta_2)\sqrt{T_{11}}}{F}, \tag{11e}$$

$$n_{11} = \frac{e^{iw/v_{c1}}\sqrt{1-L_{13}}\sqrt{1-L_{14}}N_{33}(\zeta_2)N_{33}(\zeta_1) - \sqrt{1-T_{11}}}{G}, \tag{12a}$$

$$n_{13} = -\frac{\sqrt{L_{13}}\sqrt{1-L_{14}}N_{33}(\zeta_2)\sqrt{T_{11}}}{G}, \tag{12b}$$

$$n_{14} = -\frac{\sqrt{L_{14}}\sqrt{T_{11}}}{G}, \tag{12c}$$

$$n_{21} = \frac{e^{iw/v_{c2}}\sqrt{1-L_{13}}\sqrt{1-L_{14}}N_{33}(\zeta_2)N_{34}(\zeta_1)\sqrt{T_{11}}}{G}, \tag{12d}$$

$$n_{22} = \frac{\sqrt{1-L_{14}}N_{34}(\zeta_2)\sqrt{T_{11}}}{G}. \tag{12e}$$

In the above expressions, we have introduced the definitions of F and G:

$$F = 1 - e^{i\Omega/v_{c1}}\sqrt{1-T_{11}}\sqrt{1-L_{13}}\sqrt{1-L_{14}}N_{11}(\zeta_1)N_{11}(\zeta_2), \tag{13a}$$

$$G = 1 - e^{i\Omega/v_{c1}}\sqrt{1-T_{11}}\sqrt{1-L_{13}}\sqrt{1-L_{14}}N_{33}(\zeta_1)N_{33}(\zeta_2). \tag{13b}$$

As a sufficient and necessary criterion for Gaussian entanglement states, the PPT is used to test the tripartite entanglement by the symplectic eigenvalues [26,27]. The covariance matrix of this system can be written as

$$\sigma = \begin{pmatrix} c^x_{1212} & 0 & c^x_{1221} & 0 & c^x_{1222} & 0 \\ 0 & c^y_{1212} & 0 & c^y_{1221} & 0 & c^y_{1222} \\ c^x_{2112} & 0 & c^x_{2121} & 0 & c^x_{2122} & 0 \\ 0 & c^y_{2112} & 0 & c^y_{2121} & 0 & c^y_{2122} \\ c^x_{2212} & 0 & c^x_{2221} & 0 & c^x_{2222} & 0 \\ 0 & c^y_{2212} & 0 & c^y_{2221} & 0 & c^y_{2222} \end{pmatrix}. \tag{14}$$

All the elements c^x_{pq} are the correlation coefficient between amplitude quadratures of output beams $(p,q = 12,21,22)$, while c^y_{pq} correspond to those of phase quadratures. They are defined as $c^x_{pq} = \frac{1}{2}\langle X_p X_q^* + X_p^* X_q\rangle$, $c^y_{pq} = \frac{1}{2}\langle Y_p Y_q^* + Y_p^* Y_q\rangle$ and can be calculated from Eqs. (10). A new covariance matrix σ' is given by the congruence transform $\sigma' = S^T\sigma S$, where S is the symplectic transformation,

$$S = I_1 \oplus \begin{pmatrix} \frac{1}{\sqrt{2}} & 0 & \frac{1}{\sqrt{2}} & 0 \\ 0 & \frac{1}{\sqrt{2}} & 0 & \frac{1}{\sqrt{2}} \\ \frac{1}{\sqrt{2}} & 0 & -\frac{1}{\sqrt{2}} & 0 \\ 0 & \frac{1}{\sqrt{2}} & 0 & -\frac{1}{\sqrt{2}} \end{pmatrix}, \tag{15}$$

with I_1 being the 2×2 identity matrix [28]. Generally, the positivity of the partially transposed matrix can be investigated by the smallest eigenvalue; minimum eigenvalues will show the entanglement of three modes. At first, we can focus on the first block matrix of σ' and consider the transposition of the fundamental frequency pump mode, and find the smallest one among four eigenvalues

$$E = \min\left\{\tfrac{1}{2}(c^x_{2121} + c^x_{2222} \pm \sqrt{(c^x_{2121})^2 + 4c^x_{2122}c^x_{2221} - 2c^x_{2121}c^x_{2222} + (c^x_{2222})^2}), \tfrac{1}{2}(c^y_{2121} + c^y_{2222} \pm \sqrt{(c^y_{2121})^2 + 4c^y_{2122}c^y_{2221} - 2c^y_{2121}c^y_{2222} + (c^y_{2222})^2})\right\}. \tag{16}$$

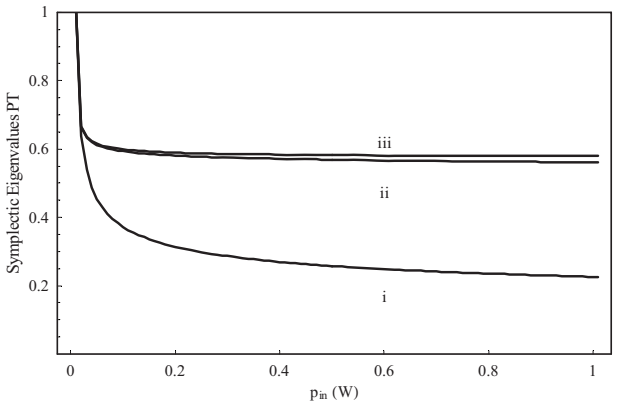

Fig. 2. Lines about symplectic eigenvalues are plotted as functions of P_{in} when $\Omega=0$. (i) Transposition of the fundamental frequency field, (ii) transposition of SH1, (iii) transposition of SH2.

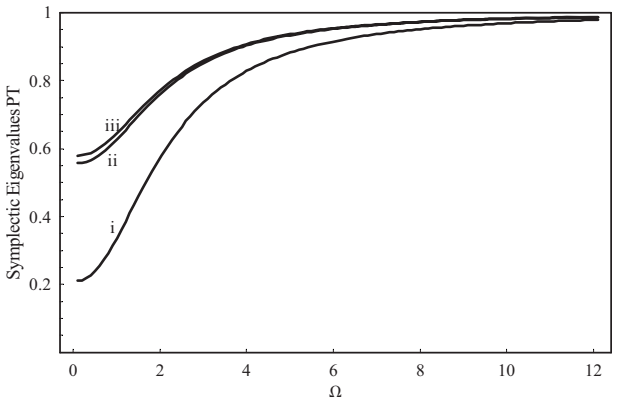

Fig. 3. Lines about symplectic eigenvalues are plotted as functions of Ω when $P_{in}=1.5$ W. (i) Transposition of the fundamental frequency field, (ii) transposition of SH1, (iii) transposition of SH2.

Then, other symplectic eigenvalues can also be simply calculated by the same way of partial transposition. Here, we choose a 1 cm length $KNbO_3$ as the nonlinear crystal and the optimum focusing is 21.1 μm as in [4]. The parameters are given as $E_{NL1}=E_{NL2}=0.015$ W^{-1}, $n_1=n_2=2.2$, $d=11$ pm/V, $T_{11}=0.01$, and $L_{13}=L_{14}=0.005$ at a fundamental wavelength of $\lambda=860$ nm. Three curves about minimum symplectic eigenvalues versus the pump power are obtained when $\Omega=0$ in Fig. 2. Here $\Omega=\omega/\nu_{ci}\gamma$ and the total loss coefficient is $\gamma=0.01$, which corresponds to $T_{11}=0.01$ and $L_{13}=L_{14}=0.005$. Three curves about minimum eigenvalues versus the analysis frequency are given when $P_{in}=1.5$ W in Fig. 3. Each curve of minimum symplectic eigenvalues in Figs. 2 and 3 corresponds to a partial transposition with respect to one of the three fields: curve i, transposition of the fundamental frequency field; curve ii, transposition of SH1; and curve iii, transposition of SH2.

It is obviously found that the all of the eigenvalue curves are below 1 in Figs. 2 and 3, demonstrating the full inseparability of the three fields. The curves vary with the pump power and analysis frequency smoothly, and the values of curve i are smaller than those of curves ii and iii. We can see that the entanglement saturates with the pump power, and the maximum entanglement is at zero analysis frequency. Besides, there is a small difference between the curves ii and iii in the range of bigger pump power or smaller analysis frequency; because of the fundamental frequency field pump depletion in the cavity, inevitably, the backward field is slightly weaker than the forward field by a small conversion between fundamental field and SHG in the first pass through the crystal [4], but it is balance for the endless input beam at the steady state condition.

In conclusion, we have theoretically demonstrated that the entanglement exists among two harmonic beams and a fundamental frequency beam generated in a frequency doubling process with a dual-port resonator. We believe that such an optical device might be used to produce four or more party entanglements. It will be very useful in the quantum information networks.

APPENDIX A: COEFFICIENTS OF MATRIX ELEMENTS AND OUTPUT QUADRATURES

The nonzero elements of the propagation matrix [4,23,24] are

$$N_{11}(\zeta)=\frac{1-\zeta\tanh\zeta}{\cosh\zeta},\quad N_{12}(\zeta)=\frac{-\sqrt{2}\tanh\zeta}{\cosh\zeta},$$

$$N_{21}(\zeta)=\frac{1}{\sqrt{2}}(\tanh\zeta+\zeta\,\mathrm{sech}^2\,\zeta),\quad N_{22}(\zeta)=\mathrm{sech}^2\,\zeta,$$

$$N_{33}(\zeta)=\mathrm{sech}\,\zeta,\quad N_{34}(\zeta)=-\frac{1}{\sqrt{2}}(\sinh\zeta+\zeta\,\mathrm{sech}\,\zeta),$$

$$N_{43}(\zeta)=\sqrt{2}\tanh\zeta,\quad N_{44}(\zeta)=1-\zeta\tanh\zeta,$$

$$\zeta_1=\sqrt{\frac{n_1}{n_2}\sqrt{\varepsilon_1 E_{NL1}p_{in}}},\quad \zeta_2=\sqrt{\frac{n_1}{n_2}\sqrt{\varepsilon_2 E_{NL2}p_{in}}}.$$

The coefficients appearing in Eqs. (9) and (10) are

$$f_{11}=\frac{e^{i\Omega/\nu_{c1}}\sqrt{T_{11}}N_{21}(\zeta_1)}{F},$$

$$f_{13}=\frac{e^{i\Omega/\nu_{c1}}\sqrt{1-T_{11}}\sqrt{L_{13}}\sqrt{1-L_{14}}N_{21}(\zeta_1)N_{11}(\zeta_2)}{F},$$

$$f_{14}=-\frac{e^{i\Omega/\nu_{c1}}\sqrt{1-T_{11}}\sqrt{L_{14}}N_{21}(\zeta_1)}{F},$$

$$f_{21}=\frac{N_{22}(\zeta_1)-e^{i\Omega/\nu_{c1}}\sqrt{1-T_{11}}\sqrt{1-L_{13}}\sqrt{1-L_{14}}N_{11}^{c2}}{F},$$

$$f_{22}=\frac{e^{i\Omega/\nu_{c1}}\sqrt{1-T_{11}}\sqrt{1-L_{14}}N_{21}(\zeta_1)N_{12}(\zeta_2)}{F},\qquad \text{(A1)}$$

where $N_{11}^{c2}=N_{11}(\zeta_2)[N_{11}(\zeta_1)N_{22}(\zeta_1)-N_{12}(\zeta_1)N_{21}(\zeta_1)]$;

$$g_{11}=\frac{e^{i\Omega/\nu_{c1}}\sqrt{T_{11}}N_{43}(\zeta_1)}{G},$$

$$g_{13} = -\frac{e^{i\Omega/\nu_{c1}}\sqrt{1-T_{11}}\sqrt{L_{13}}\sqrt{1-L_{14}}N_{43}(\zeta_1)N_{33}(\zeta_2)}{G},$$

$$g_{14} = -\frac{e^{i\Omega/\nu_{c1}}\sqrt{1-T_{11}}\sqrt{L_{14}}N_{43}(\zeta_1)}{G},$$

$$g_{21} = \frac{N_{44}(\zeta_1) - e^{i\Omega/\nu_{c1}}\sqrt{1-T_{11}}\sqrt{1-L_{13}}\sqrt{1-L_{14}}N_{33}^{c2}}{G},$$

$$g_{22} = \frac{e^{i\Omega/\nu_{c1}}\sqrt{1-T_{11}}\sqrt{1-L_{14}}N_{43}(\zeta_1)N_{34}(\zeta_2)}{G}, \quad \text{(A2)}$$

where $N_{33}^{c2}=N_{33}(\zeta_2)[N_{33}(\zeta_1)N_{44}(\zeta_1)-N_{34}(\zeta_1)N_{43}(\zeta_1)]$;

$$h_{11} = \frac{e^{i\Omega/\nu_{c1}}\sqrt{T_{11}}\sqrt{1-L_{13}}N_{11}(\zeta_1)N_{21}(\zeta_2)}{F},$$

$$h_{13} = -\frac{\sqrt{L_{13}}N_{21}(\zeta_2)}{F},$$

$$h_{14} = -\frac{e^{i\Omega/\nu_{c1}}\sqrt{1-T_{11}}\sqrt{1-L_{13}}\sqrt{L_{14}}N_{11}(\zeta_1)N_{21}(\zeta_2)}{F},$$

$$h_{21} = \frac{\sqrt{1-L_{13}}N_{12}(\zeta_1)N_{21}(\zeta_2)}{F},$$

$$h_{22} = \frac{N_{22}(\zeta_2) - e^{i\Omega/\nu_{c1}}\sqrt{1-T_{11}}\sqrt{1-L_{13}}\sqrt{1-L_{14}}N_{11}^{c1}}{F}, \quad \text{(A3)}$$

where $N_{11}^{c1}=N_{11}(\zeta_1)[N_{11}(\zeta_2)N_{22}(\zeta_2)-N_{12}(\zeta_2)N_{21}(\zeta_2)]$; and

$$k_{11} = \frac{e^{i\Omega/\nu_{c1}}\sqrt{T_{11}}\sqrt{1-L_{13}}N_{33}(\zeta_1)N_{43}(\zeta_2)}{G},$$

$$k_{13} = -\frac{\sqrt{L_{11}}N_{43}(\zeta_2)}{G},$$

$$k_{14} = -\frac{e^{i\Omega/\nu_{c1}}\sqrt{1-T_{11}}\sqrt{1-L_{13}}\sqrt{L_{14}}N_{33}(\zeta_1)N_{43}(\zeta_2)}{G},$$

$$k_{21} = \frac{\sqrt{1-L_{13}}N_{34}(\zeta_1)N_{43}(\zeta_2)}{G},$$

$$k_{22} = \frac{N_{44}(\zeta_2) - e^{i\Omega/\nu_{c1}}\sqrt{1-T_{11}}\sqrt{1-L_{13}}\sqrt{1-L_{14}}N_{33}^{c1}}{G}, \quad \text{(A4)}$$

where $N_{33}^{c1}=N_{33}(\zeta_1)[N_{33}(\zeta_2)N_{44}(\zeta_2)-N_{34}(\zeta_2)N_{43}(\zeta_2)]$.

ACKNOWLEDGMENTS

The authors would like to thank Professor Jing Zhang and Professor Changde Xie for helpful discussion. This work was supported by the National Natural Science Foundation of China (NSFC) (Grant Nos. 10774096 and 60708010), the National Basic Research Program of China (Grant No. 2010CB923102), and the Research Fund for the Returned Overseas Chinese Scholars of Shanxi Province, China.

REFERENCES

1. Z. Y. Ou, S. F. Pereira, H. J. Kimble, and K. C. Peng, "Realization of the Einstein–Podolsky–Rosen paradox for continuous variables," Phys. Rev. Lett. **68**, 3663–3666 (1992).
2. Z. Y. Ou, S. F. Pereira, and H. J. Kimble, "Realization of the Einstein–Podolsky–Rosen paradox for continuous variables in nondegenerate parametric amplification," Appl. Phys. B **55**, 265–278 (1992).
3. W. P. Bowen, R. Schnabel, P. K. Lam, and T. C. Ralph, "Experimental investigation of criteria for continuous variable entanglement," Phys. Rev. Lett. **90**, 043601 (2003).
4. O.-K. Lim and M. Saffman, "Intensity correlations and entanglement by frequency doubling in a two-port resonator," Phys. Rev. A **74**, 023816 (2006).
5. O.-K. Lim, B. Bol, and M. Saffman, "Observation of twin beam correlations and quadrature entanglement by frequency doubling in a two-port resonator," EPL **78**, 40004 (2007).
6. A. Furusawa, J. L. Sørensen, S. L. Braunstein, C. A. Fuchs, H. J. Kimble, and E. S. Polzik, "Unconditional quantum teleportation," Science **282**, 706–709 (1998).
7. W. P. Bowen, N. Treps, B. C. Buchler, R. Schnabel, T. C. Ralph, H.-A. Bachor, T. Symul, and P. K. Lam, "Experimental investigation of continuous-variable quantum teleportation," Phys. Rev. A **67**, 032302 (2003).
8. T. C. Zhang, K. W. Goh, C. W. Chou, P. Lodahl, and H. J. Kimble, "Quantum teleportation of light beams," Phys. Rev. A **67**, 033802 (2003).
9. X. Li, Q. Pan, J. Jing, J. Zhang, C. Xie, and K. Peng, "Quantum dense coding exploiting a bright Einstein–Podolsky–Rosen beam," Phys. Rev. Lett. **88**, 047904 (2002).
10. Ch. Silberhorn, N. Korolkova, and G. Leuchs, "Quantum key distribution with bright entangled beams," Phys. Rev. Lett. **88**, 167902 (2002).
11. G. M. D'Ariano, P. Lo Presti, and M. G. A. Paris, "Using entanglement improves the precision of quantum measurements," Phys. Rev. Lett. **87**, 270404 (2001).
12. P. van Loock and S. L. Braunstein, "Multipartite entanglement for continuous variables: A quantum teleportation network," Phys. Rev. Lett. **84**, 3482–3485 (2000).
13. M. Murao, D. Jonathan, M. B. Plenio, and V. Vedral, "Quantum telecloning and multiparticle entanglement," Phys. Rev. A **59**, 156–161 (1999).
14. P. van Loock and S. L. Braunstein, "Telecloning of continuous quantum variables," Phys. Rev. Lett. **87**, 247901 (2001).
15. J. Zhang, C. Xie, and K. Peng, "Controlled dense coding for continuous variables using three-particle entangled states," Phys. Rev. A **66**, 032318 (2002).
16. J. Jing, J. Zhang, Y. Yan, F. Zhao, C. Xie, and K. Peng, "Experimental demonstration of tripartite entanglement and controlled dense coding for continuous variables," Phys. Rev. Lett. **90**, 167903 (2003).
17. J. Guo, H. Zou, Z. Zhai, J. Zhang, and J. Gao, "Generation of continuous-variable tripartite entanglement using cascaded nonlinearities," Phys. Rev. A **71**, 034305 (2005).
18. A. S. Villar, M. Martinelli, C. Fabre, and P. Nussenzveig, "Direct production of tripartite pump-signal-idler entanglement in the above-threshold optical parametric oscillator," Phys. Rev. Lett. **97**, 140504 (2006).
19. S. Zhai, R. Yang, D. Fan, J. Guo, K. Liu, J. Zhang, and J. Gao, "Tripartite entanglement from the cavity with second-

order harmonic generation," Phys. Rev. A **78**, 014302 (2008).
20. S. Zhai, R. Yang, K. Liu, H. Zhang, J. Zhang, and J. Gao, "Bright two-color tripartite entanglement with second harmonic generation," Opt. Express **17**, 9851–9857 (2009).
21. A. S. Coelho, F. A. S. Barbosa, K. N. Cassemiro, A. S. Villar, M. Martinelli, and P. Nussenzveig, "Three-color entanglement," Science **326**, 823–826 (2009).
22. N. B. Grosse, S. Assad, M. Mehmet, R. Schnabel, T. Symul, and P. K. Lam, "Observation of entanglement between two light beams spanning an octave in optical frequency," Phys. Rev. Lett. **100**, 243601 (2008).
23. Z. Y. Ou, "Propagation of quantum fluctuations in single-pass second-harmonic generation for arbitrary interaction length," Phys. Rev. A **49**, 2106–2116 (1994).
24. R. D. Li and P. Kumar, "Quantum-noise reduction in traveling-wave second-harmonic generation," Phys. Rev. A **49**, 2157–2166 (1994).
25. M. K. Olsen, "Continuous-variable Einstein–Podolsky–Rosen paradox with traveling-wave second-harmonic generation," Phys. Rev. A **70**, 035801 (2004).
26. R. Simon, "Peres–Horodecki separability criterion for continuous variable systems," Phys. Rev. Lett. **84**, 2726–2729 (2000).
27. R. F. Werner and M. M. Wolf, "Bound entangled Gaussian states," Phys. Rev. Lett. **86**, 3658–3661 (2001).
28. D. Daems, F. Bernard, N. J. Cerf, and M. I. Kolobov, "Tripartite entanglement in parametric down-conversion with spatially structured pump," J. Opt. Soc. Am. B **27**, 447–451 (2010).